Advances in Applied Mathematics and Mechanics
Adv. Appl. Math. Mech., Vol. **1**, No. 3, pp. 402-414 (2009)

June 2009

Adaptive Optimal Control of the Flapping Rule of a Fixed Flapping Plate

Chui-Jie Wu[1,*] and Liang Wang[2]

[1] *School of Aeronautics and Astronautics, Dalian University of Technology, Dalian 116024, China,*

[2] *Research Center for Fluid Dynamics, PLA University of Science and Technology, Nanjing 211101, China.*

Received 29 December 2008; Accepted (in revised version) 11 February 2009

Available online 22 April 2009

Abstract. In this paper, with the use of the moving boundary computational fluid dynamics method, we developed a new real-time optimal control method which can be used to find the optimal flapping mode of a fixed flapping plate. The results show that there is a 54.0% increase in the thrust obtained by the unsteady optimal flapping rule. In addition, to reduce the cost of computation and to have a better understanding of the flapping rule, the maximum velocity at the end tip of the flapping plate is taken as the objective functional, with which the thrust is increased by 22.9%.

AMS subject classifications: 76D55

Key words: Flapping rule, optimal control, moving boundary CFD method.

1 Introduction

The Nature creates millions of strange creatures during the billions years of evolution, and every day these living creatures move around the world in their graceful, unique and the most energy saving way. But up to now, very little has been known about the mechanism of fluid mechanics of various unsteady boundary motions, such as the moving body surface, associated with the locomotion of these creatures. We hope to better understand the inscrutability of animal motion by means of studying the unsteady optimal control of the adaptive smart surface in complex flows.

On the other hand, in the community of fluid mechanics, the techniques of unsteady control and flow control with compliant surface are attracting researchers attentions. The rapid development of MEMS, MAFC and smart materials, such as the

*Corresponding author.
URL: `http://turbulence.kmip.net/`
Email: cjwudut@dlut.edu.cn (C. J. Wu), wangliang49101@163.com (L. Wang)

shape memory alloy, makes the dream of control of fluid motion with an optimal surface to come true.

As the first step, we study the optimal flapping rule of a flapping plate, to find the optimal motion mode. A new real-time optimal control method, which is applied to adaptively control of the flapping rule of a fixed flapping plate, is developed. In addition, in order to reduce the cost of computation and deepen the understanding of the optimal flapping rule, we take the maximum velocity at the end tip of the plate as the objective functional and optimize the rule directly. A relevant study of self-propelled swimming of a fish and fish school can be found in [1].

2 Numerical method and the algorithm of optimal control

2.1 Numerical algorithm and code verifications

We used the finite-volume method provided by Ferziger & Peric [2] to solve the two-dimensional version of the incompressible Navier-Stokes and continuity equations, in the following Cartesian-component (i=1, 2) integral form,

$$\frac{\partial}{\partial t}\int_\Omega \rho u_i \mathrm{d}\Omega + \int_S \rho u_i u_n \mathrm{d}S = \int_S \tau_{ij} n_j \mathrm{d}S - \int_S p n_i \mathrm{d}S, \tag{2.1}$$

$$\int_S \rho u_n \mathrm{d}S = 0, \tag{2.2}$$

where τ_{ij} is the viscous stress tensor. A second-order implicit three-time-level scheme was used for integration in time. The surface integral in (2.1) is split into four control volume (CV) face integrals approximated by the midpoint rule. As a result, the spatial precision of the algorithm is of second order.

When the cell faces move, the conservation of mass (and all other conserved quantities) is not necessarily ensured if the grid velocities are used to calculate the mass fluxes. Mass conservation can be obtained by enforcing the so-called *space conservation law*, which can be thought of as the continuity equation for zero fluid velocity:

$$\frac{\mathrm{d}}{\mathrm{d}t}\int_\Omega \mathrm{d}\Omega - \int_S \vec{u}_b \cdot \vec{n}\, \mathrm{d}S = 0, \tag{2.3}$$

where $\vec{u}_b$ is the velocity of CV cell. This equation describes the conservation of space when the CV changes its shape and/or position with time. In discretized form, (2.3) reads

$$\frac{(\Delta\Omega)^{n+1} - (\Delta\Omega)^n}{\Delta t} = \sum_c (\vec{u}_b \cdot \vec{n})_c S_c, \qquad c = e,\ w,\ n,\ s, \tag{2.4}$$

where e, w, n, and s stand for the right, left, top and bottom faces of the cell, respectively. For the implicit Euler scheme, the discretized continuity equation becomes

$$\frac{(\rho\Delta\Omega)^{n+1} - (\rho\Delta\Omega)^n}{\Delta t} + \sum_c \dot{m}_c = 0\,, \qquad c = e,\ w,\ n,\ s, \tag{2.5}$$

Table 1: Comparison of several results for cylinder flow at $Re = 100$.

	St_d	C_d (avg)	C_l (rms)
Current study	0.178	1.490	0.261
Lai & Peskin [4]	0.165	1.4473	0.3299
Dias & Majumdar [3]	0.171	1.395	0.283
Kim, Kim & Choi [5]	0.165	1.33	—
Zdravkovich [6]	0.165	1.40	—

where $\dot{m}_c$ is the mass flux through a cell face 'c'. The unsteady term has to be treated in a way consistent with the space conservation law. For incompressible flows, the contribution of the grid movement to the mass fluxes has to cancel the unsteady term so that (2.2) is satisfied in the moving grid system. The validation and details of the algorithm can be found in [2], which contains standard convergence and grid refinement tests for similar bluff-body flow, as shown in [2], p. 253.

For flow over the cylinder at Re=100, Table 1 compares the result obtained by this numerical algorithm and those from experiment and other numerical simulations, indicating that our result is reasonably good. While our computed St_d is somewhat larger than most results in the table, it is quite close to the numerical result of Dias & Majumdar [3].

It is important to understand the effect of variation of flow parameters with different numbers of grids on the surface of flapping plate. Two sets of grids are used to compute the flow parameters of a NACA0012 airfoil at Re_c=1000, α=12^o. As shown in Figs. 1 and 2, in the direction of $\vec{j}$ the grids distributed unevenly, and the grid numbers for Grid-1 and Grid-2 are 240 $\times$ 40 and 340 $\times$ 40, respectively. There are 100 and 200 grid points on the surface of the airfoil, respectively.

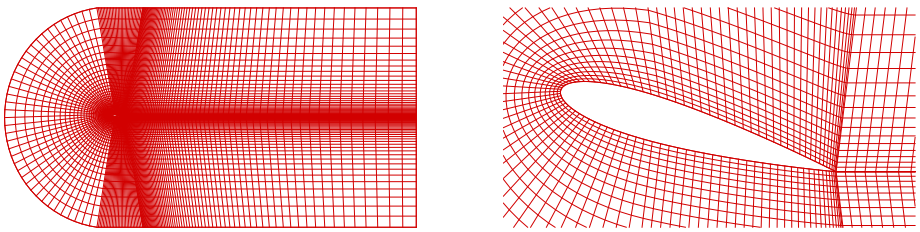

(a). Grid 1 (b). Local magnification

Figure 1: Grid 1 (240 $\times$ 40) and its local magnification.

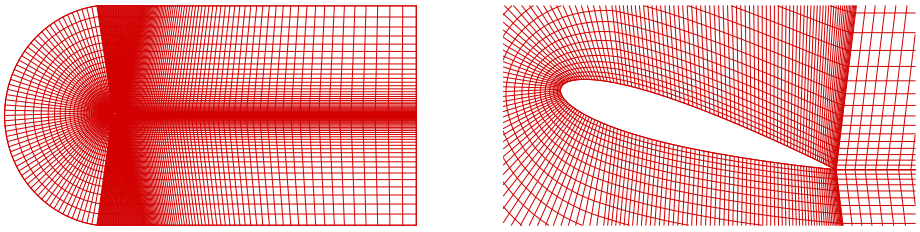

(a). Grid 2 (b). Local magnification

Figure 2: Grid 2(340 $\times$ 40) and local magnification.

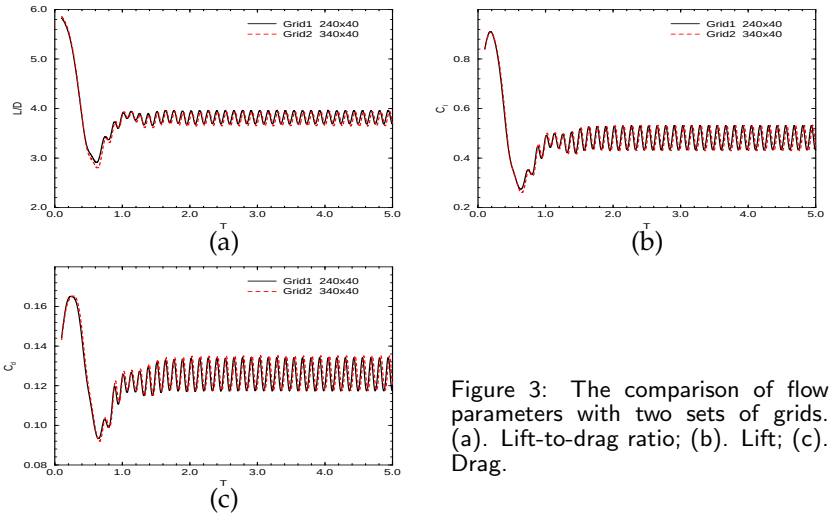

Figure 3: The comparison of flow parameters with two sets of grids. (a). Lift-to-drag ratio; (b). Lift; (c). Drag.

Fig. 3 presents the flow parameters for the two grids. It is observed that the differences between the flow parameters obtained are not big, but the time needed in the simulation of flow with Grid-2 is several times longer than that with Grid-1. Therefore, the grid number used in the simulation is 240×40.

2.2 The optimization method and its verification

The optimization method used in this study solves nonlinearly constrained minimax problems [7]. The problem to be solved is the following. Let m_1,m_2,m_3 be integers with $0 \leq m_1 \leq m_2 \leq m_3$, f_i be given real numbers, and g_i be given smooth functions. We wish to

$$\begin{cases} \min\ \omega, & \\ |f_i - g_i(x_1, \cdots, x_n)| \leq \omega, & 1 \leqslant i \leqslant m_1, \\ g_i(x_1, \cdots, x_n) \leq \omega, & m_1 + 1 \leqslant i \leqslant m_2, \\ g_i(x_1, \cdots, x_n) \leq 0, & m_2 + 1 \leqslant i \leqslant m_3, \end{cases} \tag{2.6}$$

by selecting the optimal values of $x_1, \cdots, x_n$.

In order to verify the reliability of this optimization method, the following optimization problem is chosen and solved with the method in [8]:

$$\min\ f(\vec{x}) = (x_1 - x_4)^2 + (x_2 - x_5)^2 + (x_3 - x_6)^2, \tag{2.7}$$

which is subject to the constrain conditions

$$\begin{cases} 5 - x_1^2 - x_2^2 - x_3^2 \geqslant 0, \\ 1 - (x_4 - 3)^2 - x_5^2 \geqslant 0, \\ 8 - x_6 \geqslant 0, \\ x_6 - 4 \geqslant 0. \end{cases} \tag{2.8}$$

The exact solution for (2.7) – (2.8) is $\vec{x}^*$=$(1, 0, 2, 2, 0, 4)$, and the corresponding optimal

Table 2: The comparison between approximate and exact solutions. V: variables; IV: initial values; OFV: objective functional values; N: numbers of iteration; ES: exact solution.

V	IV	Analytical derivate	Difference derivate	ES
x_1	1.0	0.99999999790387E+00	0.99999991804778E+00	1.0
x_2	1.0	-0.49112942115734E-08	-0.46570133988029E-10	0.0
x_3	1.0	0.20000000410220E+01	0.20000000410220E+01	2.0
x_4	3.0	0.19999999999855E+01	0.19999999999615E+01	2.0
x_5	0.0	-0.466916224982010E-08	-0.385890276931850E-08	0.0
x_6	5.0	0.40000000000000E+01	0.39999999997850E+01	4.0
OFV	21.0	0.49999999998910E+01	0.49999999988800E+01	5.0
N	-	40	55	-

index is $f(\vec{x}^*)$ =5. In the optimization process, it is needed to find the derivatives of object functional and the constrain condition. There are two ways to get the derivatives, i.e., using the analytical derivative expression and the middle point difference formula of the code, which is

$$\frac{\partial f}{\partial x_i} = \frac{1}{2h}\Big[f(x_1, \cdots, x_i + h, \cdots, x_n) - f(x_1, \cdots, x_i - h, \cdots, x_n)\Big]. \tag{2.9}$$

In many optimization problems, it is very difficult to give the explicit expression of the object functional and the constrain condition. Therefore, the second method is widely used in practice. From Table 2, one can find that the results obtained by both methods are very close to each other, with the errors below 10^{-8}.

2.3 The procedure of unsteady optimal control

The procedure of unsteady optimal control is as follows:

1. Select parameters to be optimized and determine their initial values $\vec{x_0}$;
2. Compute the flow field on the initial grid till t_0, at which the process of control start;
3. Save the flow field, the lift F_y^0 and the thrust F_x^0 at t_0. Calculate the value of the objective functional $J(\vec{x_0})$;
4. Find a search step $\vec{h}$ and reconstruct the new flapping rule with $\vec{x_0} + \vec{h}$;
5. Create new grids with the new rule. Then, interpolate the flow field at t_0 into the new grids to get the new initial field.
6. Use the new grids and the new initial field to compute the flow field at $t_0 + \mathrm{d}t$ ($\mathrm{d}t$ is the time step) and the value of objective functional $J(\vec{x_0} + \vec{h})$;
7. If $J(\vec{x_0} + \vec{h}) < J(\vec{x_0})$ and all of the constrains are satisfied, let $\vec{x_0} = \vec{x_0} + \vec{h}$, and $J(\vec{x_0}) = J(\vec{x_0} + \vec{h})$;
8. The process of optimization will be stopped if the value of objective functional can not be reduced anymore and the process of 3-7 will be repeated otherwise.
9. Compute the flow field on the new grids corresponding to the optimized rule till $t_0 + \Delta t$ ($\Delta t \gg \mathrm{d}t$) at which the next control starts;
10. The program will be stopped if the terminal condition is satisfied and let $t_0 = t_0 + \Delta t$; otherwise repeat 3-9.

3 Numerical results

Here, we apply the above moving boundary CFD and the optimal control methods in the study of unsteady optimal control of the flapping rule, in order to get the maximum thrust with an unchanged flapping frequency. Since we want to obtain the unsteady optimal flapping rule, i.e., the optimal flapping rule is changed with time and flow condition, the history of flow will be effected to the resulting unsteady optimal flapping rule, therefore it is much more difficult than the usual optimization, in which the flow history dose not influence the result.

3.1 Numerical simulation of a flapping plate

In this paper, both simulation and control are based on the flapping rule [9] which is the result obtained by fitting the swimming motion of a real fish. The rule of the centerline of the fish body is

$$H(x,t) = h_1(x)\cos\{\omega[t-k_1(x)]\} + h_3(x)\cos\{3\omega[t-k_3(x)]\} + h_5(x)\cos\{5\omega[t-k_5(x)]\}, \tag{3.1}$$

where

$$\begin{cases} h_1(x) = -0.073 + 0.093/(x+1.0) + 0.125x^2, \\ h_3(x) = 0.001 + 0.001x^3 + 0.005x^{10}, \\ h_5(x) = 0.005 - 0.002x^3 + 0.003x^{10}, \\ k_1(x) = -1.392x + 2.281\sin(x) - 0.985\cos(x), \\ k_3(x) = 2.781x - 3.102\sin(x) - 0.119\cos(x), \\ k_5(x) = -0.215 + 0.304x^2 + 0.028\cos(10.0x). \end{cases} \tag{3.2}$$

The distribution of the thickness of the plate is the same as NACA0012. In one period, the process of flapping is shown in Fig. 4 by solid lines.

C-type grids of total 240×40 are used. The flapping period of plate is T=1.0. The inflow velocity is u_0=0.05. The kinematic viscosity coefficient is $\nu = 1.5 \times 10^{-5}$. We take the projected length of plate in x-direction as chord and its value is c=0.1 in the computational domain. Therefore, the Reynolds number based on the chord is Re_c=333. In addition, the thrust is defined as the negative value of the total force in x-direction. If inflow velocity is small, the main part of thrust will be positive.

For the boundary conditions, on the moving surface of flapping plate, the non-slip boundary condition is applied, on which the velocities are obtained from the optimal control process; The left boundary is an inflow boundary. The right, top and bottom boundaries are continuous outflow boundaries. For the initial condition, set the velocity of the whole field to be $\vec{u}$=0.05$\vec{i}$, where $\vec{i}$ is the unit vector at x-direction.

Fig. 5 shows the vorticity field and the vectors represent the relative velocity field from which the averaged flow has been removed in one period. It can be seen that the reverse Kármán vertex street is created and developed.

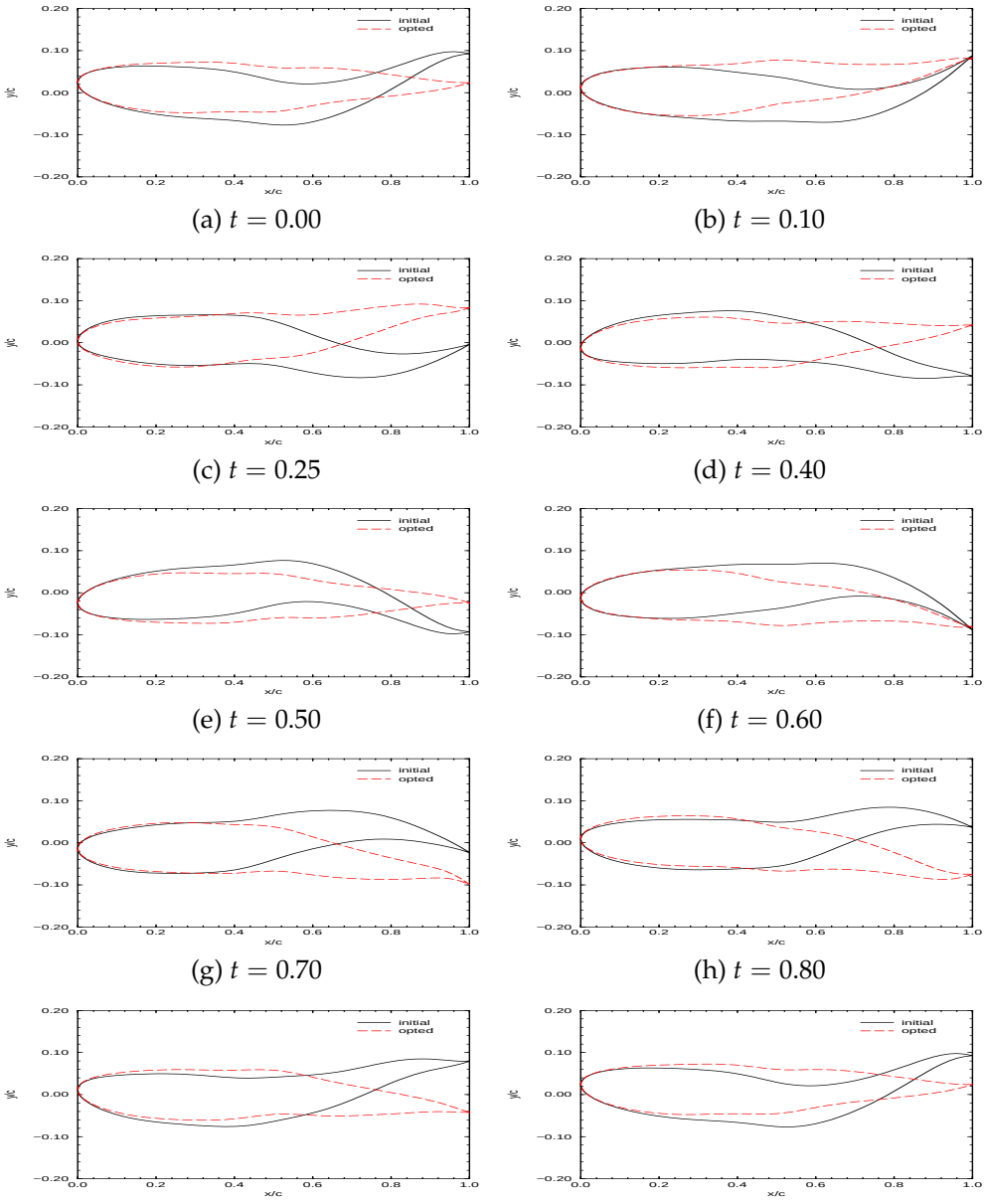

(a) $t = 0.00$ (b) $t = 0.10$

(c) $t = 0.25$ (d) $t = 0.40$

(e) $t = 0.50$ (f) $t = 0.60$

(g) $t = 0.70$ (h) $t = 0.80$

(i) $t = 0.90$ (j) $t = 1.00$

Figure 4: Comparing of flapping processes before and after the unsteady optimization in one period.

3.2 Unsteady optimization of flapping rule

In order to increase the thrust under the condition of a fixed flapping frequency, the flapping rule is dynamically optimized. The flapping rule of the plate's centerline is the same as (3.1); $h_1(x), h_3(x), h_5(x)$ are the same as (3.2), but $k_1(x), k_3(x), k_5(x)$ in (3.2)

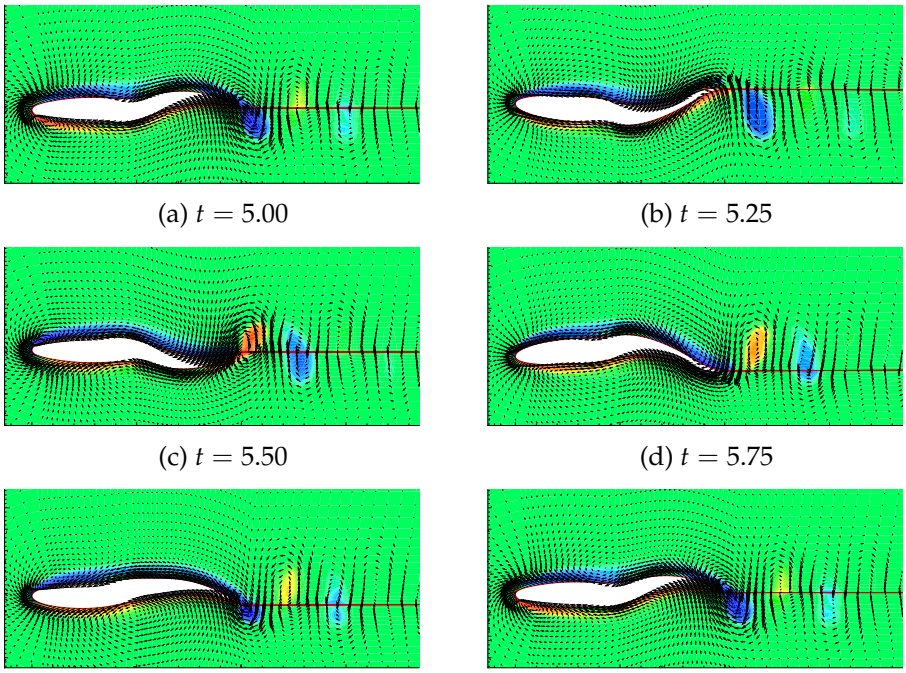

(a) $t = 5.00$ (b) $t = 5.25$

(c) $t = 5.50$ (d) $t = 5.75$

(e) $t = 5.90$ (f) $t = 6.00$

Figure 5: Test 3.1: Vorticity field and relative velocity field with the original rule in one period.

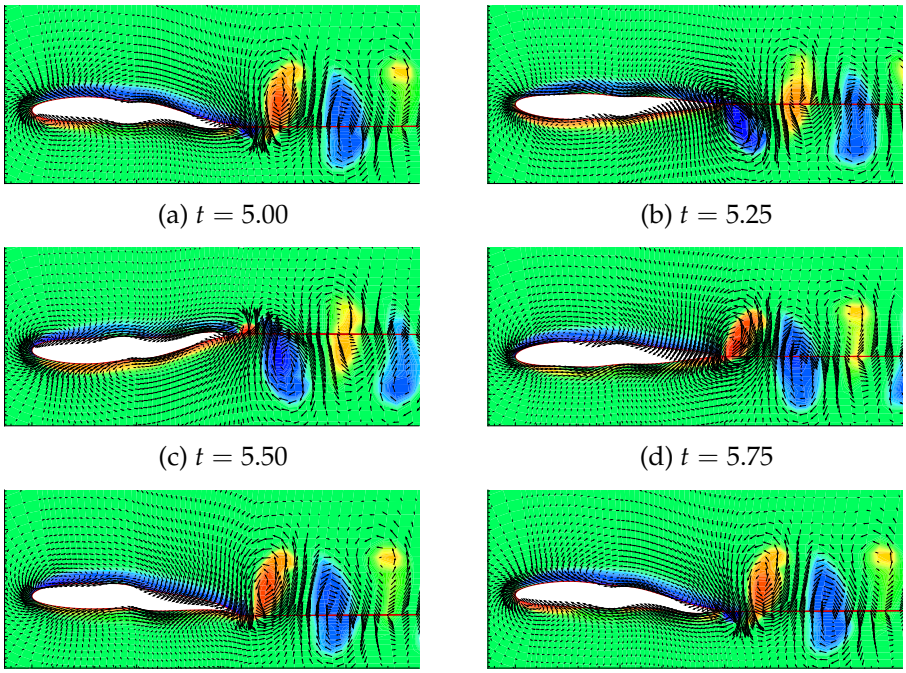

(a) $t = 5.00$ (b) $t = 5.25$

(c) $t = 5.50$ (d) $t = 5.75$

(e) $t = 5.90$ (f) $t = 6.00$

Figure 6: Test 3.2: Vorticity field and relative velocity field with the optimized rule in one period.

are replaced by

$$\begin{cases} k_1(x) = P_1 x + 2.281\sin(x) - 0.985\cos(x), \\ k_3(x) = 2.781x + P_2\sin(x) - 0.119\cos(x), \\ k_5(x) = -0.215 + P_3 x^2 + 0.028\cos(10.0x), \end{cases} \tag{3.3}$$

where P_1, P_2 and P_3 are parameters to be optimized, which may not be unique, i.e., one can chose others to do the optimal control. Chose the initial values for P_1, P_2 and P_3 as

$$P_1^0 = -1.392, \quad P_2^0 = -3.102 \quad \text{and} \quad P_3^0 = 0.304.$$

In order to obtain the maximum thrust, following objective functional is used:

$$J = \frac{|F_y - F_y^0|}{|F_y^0|} + 10\frac{F_x}{|F_x^0|}. \tag{3.4}$$

To reduce J, the total force in the y-direction (lift) should be constrained and the total force in the x-direction should be decreased as much as possible. The constraint is $\Delta y_{max}<0.002$, where Δy_{max} is the maximum displacement of the centerline within one step of optimization.

The total computational time is 15, and the optimization time step is Δt=0.03. Fig. 7 shows the history of thrust in unsteady optimization process. It can be seen that both the maximum and the minimum of the thrust are increased continually. When

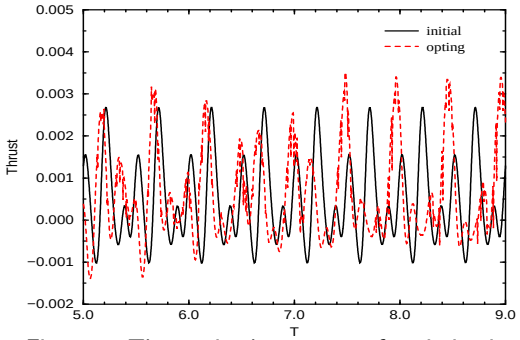

Figure 7: Thrusts in the process of optimization.

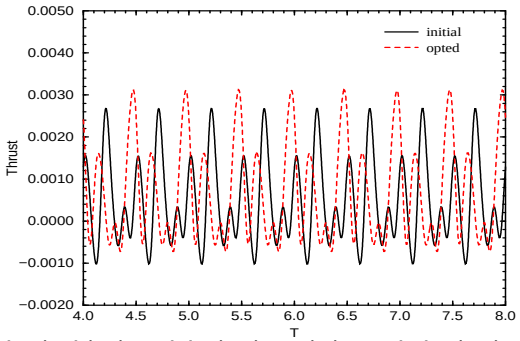

Figure 8: Thrusts obtained with the original rule and the optimized rule (unsteady optimization).

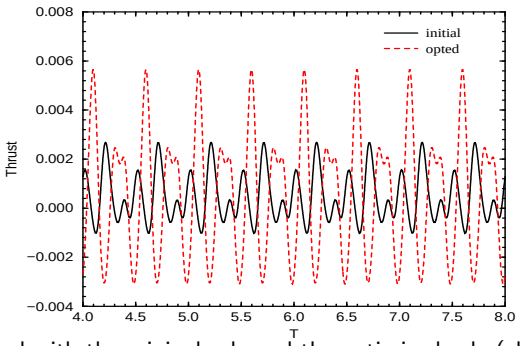

Figure 9: Thrusts obtained with the original rule and the optimized rule (characteristic optimization).

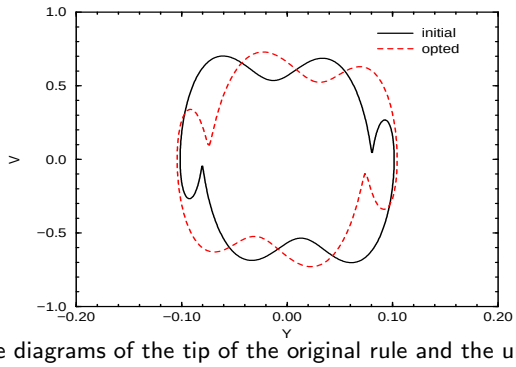

Figure 10: The phase diagrams of the tip of the original rule and the unsteady optimized rule.

$t>8$, the peak of thrust is almost fixed. Therefore, we take the rule at t=7.95 to do the simulation again, and compare the results with the original ones.

At t=7.95, the three optimized parameters are P_1=−2.178, P_2=−3.098 and P_3= 0.398. The dashed line in Fig. 4 shows the process of flapping controlled by the optimization rule. Comparing it with the solid line, it can be seen that the flapping rule has been changed greatly. Some wavy motion are overlapped to the surface of the plate. Fig. 6 shows that the reverse Kármán vertex street is strengthened remarkably; therefore the thrust is increased. From Fig. 10, it can be seen that the phase diagram of the end tip of plate has been changed greatly, but the needed power is not changed much. Fig. 8 shows the thrust with the optimized rule. There is a 54.0% increase in average value of the thrust. Therefore, the new rule, which is the combination of flapping and wavy motion, can increase the flapping efficiency at the unchanged flapping frequency. This result is particularly interesting since it is known that a prior designed moving wavy wall can be used in the drag reduction flow control [10], but the wavy motion in this study is the result of optimal control of the flapping rule.

3.3 Characteristic optimization of flapping rule of the plate

In the last section, the thrust is increased greatly with the method of unsteady optimization of the flapping rule of the plate. In the process of optimization, the Navier-Stokes equations have to be solved several thousand times repeatly. Therefore, the

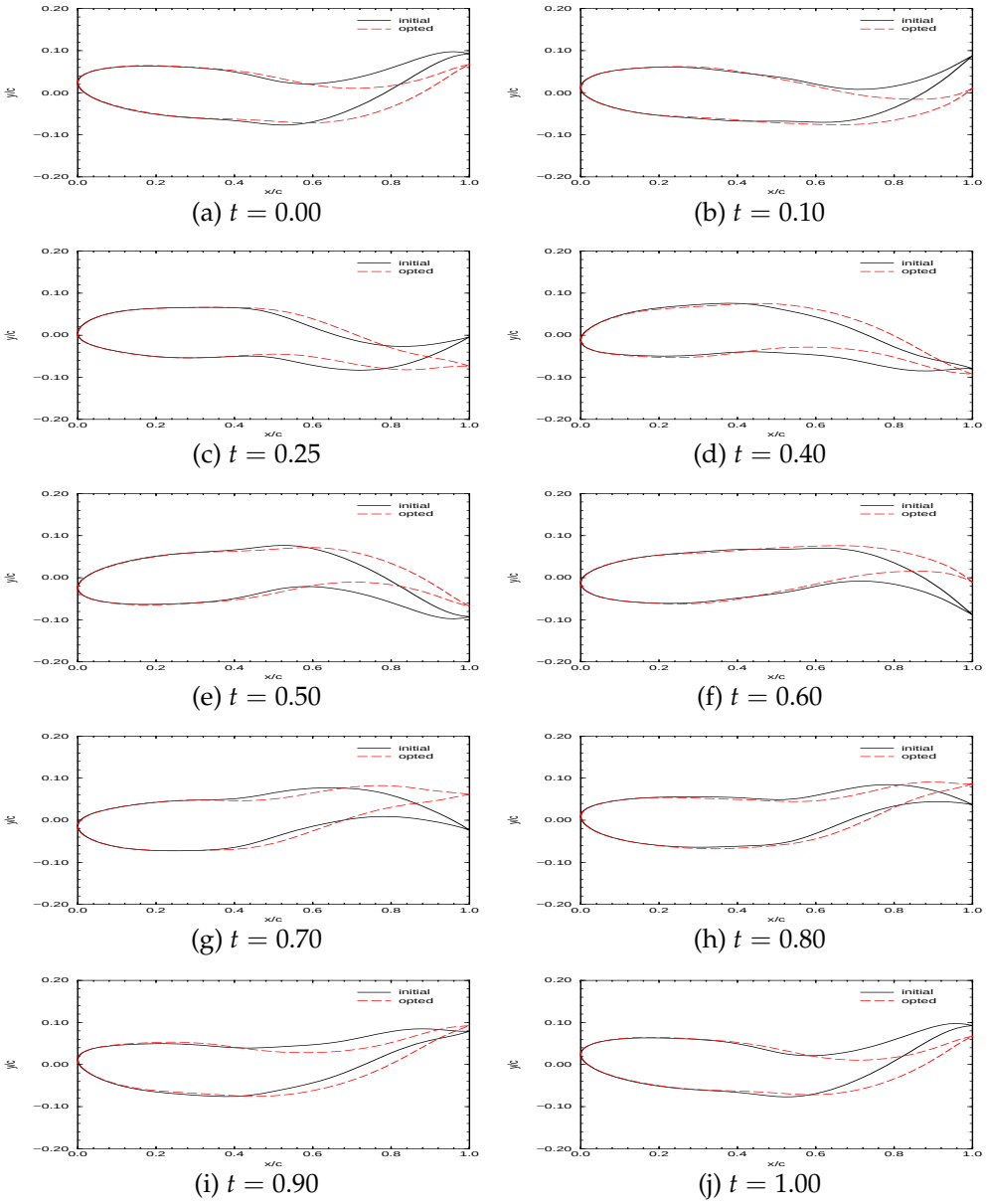

(a) $t = 0.00$ (b) $t = 0.10$

(c) $t = 0.25$ (d) $t = 0.40$

(e) $t = 0.50$ (f) $t = 0.60$

(g) $t = 0.70$ (h) $t = 0.80$

(i) $t = 0.90$ (j) $t = 1.00$

Figure 11: Flapping processes with original rule and characteristic optimized rule in one period.

total computational time is very long. In this section, first, we compare the original rule with the unsteady optimized one. The purpose is to find some characteristic parameters. Then, we will take these parameters as objects and optimize the rule directly. As a result, the cost of computation is reduced, but the efficiency of flapping is still increased compared with the oringial one.

Let us first check the velocity and amplitude of the end tip of plate. Fig. 10 shows the phase diagram of the original rule and the unsteady optimized rule. From the fig-

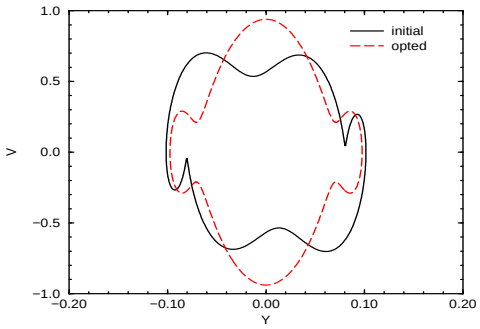

Figure 12: The phase diagrams of the tip of the original rule and the characteristic optimized rule.

ure, it can be seen that both the maximum velocity and the amplitude are increased. As a test, we take the maximum velocity of the tip as the object in the direct optimization. The objective functional is

$$J = -|v_{tail}|. \tag{3.5}$$

Because the analytic function of flapping rule is known, velocity can be calculated easily. As in the last section, we take the same three parameters in (3.3) as optimal parameters, and initial values and optimal algorithm are the same. In such way, in the direct optimization of the maximum velocity of the tip, only a few seconds are needed to get the result, and the following three optimized parameters P_1=−1.5262, P_2=−2.7995 and P_3=0.0995, are obtained.

As shown in Fig. 11, the flapping mode of characteristic optimized rule is not changed too much compared with the original one. Fig. 12 shows the phase diagrams of the tip of the original rule and the characteristic optimized rule. It is seen that the peak of the maximum velocity is increased greatly, and the amplitude is decreased slightly and becomes symmetrical. The difference of flapping modes between the original rule and the unsteady optimized rule exist all over the plate. But the main difference between the original rule and the characteristic optimized rule only lies at the end tip of plate. Fig. 9 shows the thrusts of the original rule and the characteristic optimized rule. Compared with Fig. 8, it can be seen that the positive thrust peak of the characteristic optimized rule is the maximum of the three. However the negtive thrust peak of the characteristic optimized rule is far less than the others. Therefore, compared with the original one, there is only a 22.9% increase in thrust. The main reason is that the searching space of characteristic optimization is much smaller than that of unsteady optimization.

4 Conclusions

It is calculated that the method of unsteady optimal control can be used to optimize the flapping rule of a fixed plate. Using this method, we can get a new flapping mode which is a combination of flapping and wavy motion. The results show that the thrust

increases 54.0% with the unsteady optimized flapping rule at the same frequency. On the other hand, in order to reduce the cost of computation, we take the maximum velocity at the end tip of the plate as the objective functional in the direct optimization. As a result, there is a 22.9% increase in the thrust with this method.

Acknowledgments

The research of the authors is supported in part by the National Natural Science Foundation of China (#10532040).

References

[1] C. J. WU AND L. WANG, *Numerical simulations of self-propelled swimming of 3D bionic fish school*, Science in China (E), 52(3) (2009)pp: 658–669.
[2] J.H. FERZIGER AND M. PERIĆ, Computational Method for Fluid Dynamics, Spinger-Verlag, 1999.
[3] Y.-H. TSENG AND J. H. FERZIGER, *A ghost-cell immersed boundary method for flow in complex geometry*, J. Comput. Phys., 192 (2003), pp. 593–623.
[4] M. LAI AND C. S. PESKIN, *An immersed boundary method with formal second-order accuracy and reduced numerical viscosity*, J. Comput. Phys., 160 (2000), pp. 705–719.
[5] J. KIM, D. KIM AND H. CHOI, *An immersed-boundary finite-volume method for simulations of flow in complex geometries*, J. Comput. Phys., 171 (2000), pp. 132–150.
[6] M. M. ZDRAVKOVICH, Flow Around Circular Cylinders. Vol. 1: Fundamentals, Oxford University Press, New York, 1997.
[7] E. K. KAUFMAN, D. J. LEEMING AND G. D. TAYLOR, *An ODE-based approach to nonlinearly constrained minimal*, Numerical Algorithms, 9 (1995), pp. 25–37.
[8] Q. K. YE AND Z. M. WANG, Numerical Method for Optimization and Optimal Control, Science Press, Beijing, 1986 (in Chinese).
[9] O. K. REDINIOTIS, D. C. LAGOUDAS, T. MASHIO, L. J. GARNER AND M. A. QIDWAI, Theoretical and Experimental Investigations of an Active Hydrofoil with SMA Actuators, Internet, 2000.
[10] C. J. WU, L. WANG AND J. Z. WU, *Suppression of the von Karman vortex street behind a circular cylinder by a travelling wave generated by a flexible surface*, J. Fluid Mech., 574 (2007), pp. 365–391.